Heliyon

Received:
24 October 2017
Revised:
2 December 2017
Accepted:
17 January 2018

Cite as: Quang Hung Trinh, Md. Mokter Hossain, Seong H. Kim, Young Sun Mok. Tailoring the wettability of glass using a double-dielectric barrier discharge reactor. Heliyon 4 (2018) e00522. doi: 10.1016/j.heliyon.2018.e00522

Tailoring the wettability of glass using a double-dielectric barrier discharge reactor

Quang Hung Trinh [a], **Md. Mokter Hossain** [a], **Seong H. Kim** [b], **Young Sun Mok** [a,*]

[a] *Department of Chemical and Biological Engineering, Jeju National University, Jeju 690-756, Republic of Korea*

[b] *Department of Chemical Engineering, Pennsylvania State University, University Park, PA 16802, USA*

* Corresponding author.

E-mail address: smokie@jejunu.ac.kr (Y.S. Mok).

Abstract

A double dielectric barrier discharge reactor operated at a low power frequency of 400 Hz and atmospheric pressure was utilized for regulating the wettability of glass surface. The hydrophobic treatment was performed by plasma polymerization of tetramethylsilane (TMS, in argon gas). The obtained results showed that the TMS coatings formed on the glass substrates without oxygen addition were smooth, uniform films with the maximum water contact angle (WCA) of about 106°, which were similar to those obtained by low pressure, high power frequency plasmas reported in the literature. The addition of oxygen into TMS/Ar plasma gas decreased the WCA and induced the formation of SiOSi and/or SiOC linkages, which dominated the existence of $Si(CH_2)_nSi$ network formed in TMS/Ar (without oxygen) plasma.

Keywords: Condensed matter physics, Engineering, Materials science

1. Introduction

Non-thermal plasma (NTP) or cold plasma has been widely investigated for various applications ranging from air pollution control to material processing [1, 2, 3]. Over the past decades, the NTP technology has emerged as a new surface modification method with typical distinct advantages of quick respond without affecting the bulk properties, no chemical solvents required and no thermal

http://dx.doi.org/10.1016/j.heliyon.2018.e00522
2405-8440/© 2018 The Authors. Published by Elsevier Ltd. This is an open access article under the CC BY-NC-ND license (http://creativecommons.org/licenses/by-nc-nd/4.0/).

damages [4]. Thanks to the thermal non-equilibrium nature, NTP is suitable for treatment of a range of materials and is especially useful for those heat-sensitive. The change in surface properties, such as wettability, results from altering the surface chemistry and/or surface morphology. In plasma processes, chemical functional groups can be generated by surface modification or thin film deposition on various materials like glasses, polymers, ceramics, metalloids and also on conductive surfaces like metals [5, 6, 7]. The deposition of plasma-polymerized hexamethyldisiloxane on fabrics was successfully done to give hydrophobic self-cleaning properties [8]. Kim et al. [9] demonstrated that plasma processes can achieve hydrophobic treatments of various substrates including metallic and insulating surfaces. Besides, Barankin et al. [10] produced hydrophobic coatings on glass and acrylic surfaces by using a low-temperature atmospheric pressure plasma with a fluoroalkylsilane precursor.

Non-thermal plasma treatment of glasses has gained more attention recently. The intrinsic hydrophilic property of glass surface could be transformed to hydrophobicity (*i.e.*, water contact angle above 90°) with self-cleaning effect by plasma polymerization deposition, desirable for many products, such as windows, windshields, and solar panels, *etc*. [11, 12, 13]. Various precursors from hydrocarbons to organosilicons have been tested for NTP assisted fabrication of hydrophobic thin films. The static water contact angle (WCA) of above 150° (referred as super-hydrophobicity) for the thin films coated on the flat glass or silicon substrates using benzene/helium, benzene/argon, tetramethylsilane/helium and toluene-hexamethyldisiloxane/argon plasmas were previously reported [14, 15, 16, 17]. The glass hydrophilic treatment is, however, crucial for many subsequent operations of glass processing, for example, gluing, printing, coating, *etc*. [18]. NTP methods are recently replacing chemical methods for surface cleaning and activation because they are faster and environmentally friendly [19]. From previous studies, NTPs have been proven to be effective for improving the wettability and therefore for the surface adhesion of glasses with other materials [20, 21, 22, 23, 24].

In this work, tailoring the wettability of glass surfaces by plasma hydrophobic coating at a low power frequency of 400 Hz and atmospheric pressure was studied. A double-dielectric barrier discharge (DDBD) reactor that can produce uniform plasma at atmospheric pressure was used for hydrophobic treatment. The DDBD plasma reactor has several merits over conventional techniques such as plasma jet, microwave plasma, rf plasma, *etc*. The DDBD can cover a large surface area that make it possible for uniform coating over the surface, and consumes relatively low electric power compared to vacuum-based plasmas like rf and microwave plasmas. $SiO_xC_yH_z$ films deposited by a NTP method with their unique electronic, optoelectronic, chemical and wettability properties have been utilized in many application areas ranging from very large scale integration (VLSI) technology to

http://dx.doi.org/10.1016/j.heliyon.2018.e00522
2405-8440/© 2018 The Authors. Published by Elsevier Ltd. This is an open access article under the CC BY-NC-ND license (http://creativecommons.org/licenses/by-nc-nd/4.0/).

hydrophobic coatings [25, 26]. Tetramethylsilane (TMS) was chosen as the precursor because of its high chemical reactivity and vapor pressure (11.66 psi at 20 °C) compared to other monomers such as hexamethyldisiloxane. This helps reduce the energy consumption for plasma ignition and vaporizing precursors. In the past, polymerization of TMS was studied by many researchers, mostly under low pressure and/or radio frequency (RF) plasma conditions [25, 27, 28, 29]. The use of atmospheric and low frequency plasma could, however, avoid the system complexity and cooling, as well as reduce the power consumption. Different contents of oxygen were added to the TMS/Ar gas mixture in order to investigate the change in the wettability and chemical composition of the resulting films.

2. Experimental

2.1. Materials and experimental setup

Tetramethylsilane (≥99.0%, liquid phase) and microscope glass slides used as the substrates for coating (25.4 × 76.2 × 1 mm) were purchased from Sigma Aldrich (Germany) and Sail Brand (China), respectively. The precursor was used as received without further purification.

The experimental setup including a DDBD plasma reactor is shown in Fig. 1. The DDBD reactor with a discharge gap of 4 mm was composed of two silver paste electrodes (22 × 70 mm) coated on glass plates (78 × 173 × 1.6 mm) acting as the dielectrics. The upper electrode was connected to the high voltage (HV) terminal of an AC transformer operating at a frequency of 400 Hz. The remaining grounded electrode was connected to a capacitor (capacitance: 1.0 μF) in series in order to measure the reactor discharge power. For a purpose of eliminating oxygen from ambient air, the DDBD reactor was placed inside an insulating cylindrical chamber (inner diameter: 133 mm, length: 300 mm), which was flushed by pure Ar gas (flow rate: 1.0 L min^{-1}) for 20 min before carrying out every experiment.

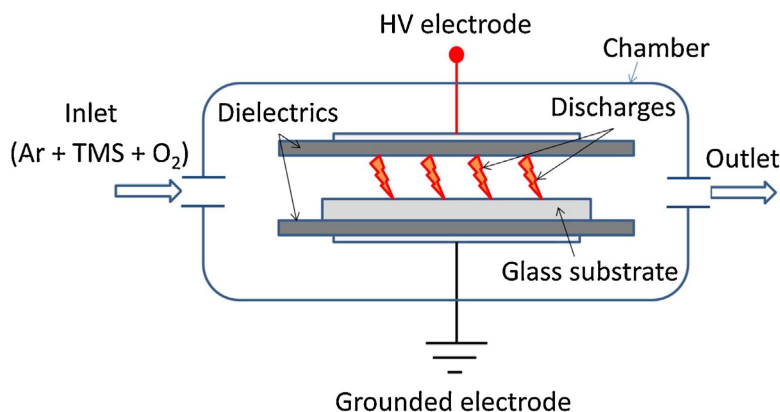

Fig. 1. Experimental setup.

http://dx.doi.org/10.1016/j.heliyon.2018.e00522
2405-8440/© 2018 The Authors. Published by Elsevier Ltd. This is an open access article under the CC BY-NC-ND license (http://creativecommons.org/licenses/by-nc-nd/4.0/).

2.2. Methods

The precursor was delivered to the reactor by bubbling liquid TMS (at 20 °C) contained in a pyrex flask using Ar gas, whose flow rate was controlled in a range of 1.6 and 18.8 mL min^{-1}, resulting in the gaseous TMS content varied from 1.3 to 15.1 mL min^{-1}. This TMS-containing gas was then mixed with a main Ar gas stream (flow rate: from 0.5 to 2.0 L min^{-1}) before entering the reactor chamber. Oxygen was also added to the gas stream in order to investigate the oxygen dependence of the wettability and chemical composition of the coatings. The utilization of O_2/Ar gas instead of air is to avoid the formation of nitrogen oxides, which are gaseous pollutants and intrinsically formed in air plasma [30, 31]. All gas flows were controlled by mass flow controllers (MFC), which were calibrated before use.

The voltage applied to the HV electrode was recorded by a digital oscilloscope (Tektronix DPO3034) via a high voltage probe (Tektronix P6015A) with an attenuation ratio of 1000:1. The electrical charge flowing through the reactor was estimated by measuring the voltage across the capacitor using a 10:1 voltage probe (Tektronix P6139B). The discharge power was then determined from the so-called voltage-charge Lissajous figures.

As aforementioned, for each experiment, the reactor chamber was first flushed with Ar gas for about 20 min to minimize the amount of pre-existing air. After that, the glass substrate was pre-treated with plasma of pure Ar (flow rate: 1.0 L min^{-1} and applied voltage: 10 kV) for 5 min. TMS or a mixture of TMS and oxygen was then added during the coating process. Finally, the coated samples were stabilized in Ar atmosphere in the reactor for 5 min without plasma ignition before being taken out for characterization.

The coating wettability was probed by measuring the static WCA using a goniometer (SEO Phonix 300, Korea) with the water drop volume of about 9 μL. For each sample, the WCA was measured at several different positions on the sample's surface. The WCA value representing for each sample is the average of several values measured along the sample's length. The WCA of the pristine glass was measured to be around 30°. It is noted that the WCA was generally measured without aging time (*i.e.*, soon after plasma treatment), unless otherwise mentioned. The chemical compositions of the deposited films were analyzed using a Fourier transform infrared spectrometer (FTIR, 7600, Lambda Scientific) and X-ray photoelectron spectroscopy (XPS, Theta Probe AR-XPS System, Thermo Fisher Scientific) with monochromatic Al Kα radiation (1488.6 eV) operated at 15 kV and a 150-W X-ray excitation source. The resolution of the FTIR was set to 1 cm^{-1}, and ten spectroscopic scans of the spectra were averaged. The surface morphology of the pristine and treated glass surfaces was probed by an atomic force microscopy (AFM, Force Precision Instrument Co., Taipei, Taiwan). The surface morphology

http://dx.doi.org/10.1016/j.heliyon.2018.e00522
2405-8440/© 2018 The Authors. Published by Elsevier Ltd. This is an open access article under the CC BY-NC-ND license (http://creativecommons.org/licenses/by-nc-nd/4.0/).

(scan area: 2.5 μm × 2.5 μm; scan rate: 0.3 Hz) was probed with a 10-nm-radius silicon tip oscillating at resonant frequency of 200 ~ 400 kHz.

3. Results and discussion

3.1. Hydrophobic treatment of glass

The hydrophobic treatment of glass surfaces with TMS was carried out without oxygen addition. Fig. 2 shows the dependence of WCA on the total gas flow rate and applied voltage. As seen from Fig. 2(a), when keeping the applied voltage, deposition time and TMS amount constant, the WCA was observed to be lower at 0.5 L min^{-1} than at the higher values of gas flow rate. This could partially result from the less stable plasma generated under the low gas flow condition. At above 0.5 L min^{-1}, the WCA remained at around 103°. For further experiments, the main gas stream was then set at 1.0 L min^{-1}, unless otherwise noted. The change in WCA with the applied voltage is shown in Fig. 2(b). In general, the measured WCA showed weak applied voltage dependence within the investigated range. Slightly increased with increasing the applied voltage from 10 to 12 kV, the WCA seemed to be stable thereafter. At 16 kV, which corresponds to a discharge power density of 0.17 W cm^{-2}, the WCA was recorded to be 98°. Hereafter, the applied voltage for TMS plasma coating was kept at 16 kV.

The change in WCA as a function of TMS concentration is shown in Fig. 3. The experiment was carried out at a deposition time of 5 min. Similar to the applied voltage, increasing the TMS content positively affected the hydrophobicity of the coating. At the TMS concentration of 0.7 v/v% or more, the WCA reached above 100°. The maximum WCA of 106° was achieved at 1.1 v/v%, corresponding to a TMS flow rate of 11.2 mL min^{-1}. This WCA is higher than or comparable to those achieved by low-pressure, RF plasmas [27, 32, 33, 34]. Similar results were also

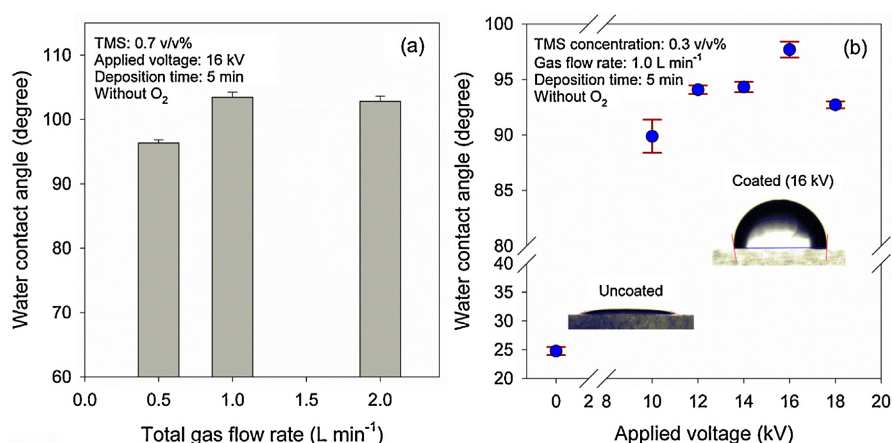

Fig. 2. Gas flow rate (a) and applied voltage (b) dependence of WCA of hydrophobically treated samples.

http://dx.doi.org/10.1016/j.heliyon.2018.e00522
2405-8440/© 2018 The Authors. Published by Elsevier Ltd. This is an open access article under the CC BY-NC-ND license (http://creativecommons.org/licenses/by-nc-nd/4.0/).

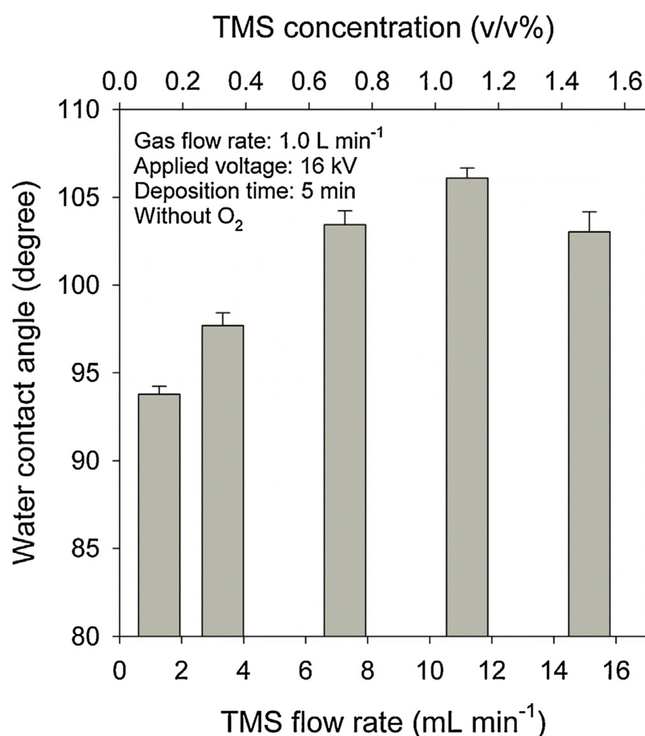

Fig. 3. TMS concentration dependence of WCA of hydrophobically treated samples (gas flow rate: 1.0 L min^{-1}, applied voltage: 16 kV, deposition time: 5 min).

previously reported by using atmospheric pressure, kHz power frequency plasma deposition on glass and PET substrates [13, 35].

Fig. 4 indicates the effect of deposition time on WCA at a TMS concentration of 0.7 v/v%. The WCA sharply increased from about 30° (for pristine glass) to 98° after only 5 s of treatment, showing a quick response of the surface hydrophobicity to the plasma treatment. After that, the WCA gradually increased with the increase of deposition time. Further raising the treatment period over 300 s, however, caused a slight decrease in WCA. The samples after treatment were stored in closed conical tubes. Fig. 5 shows the WCA of the 5-min-coated sample with respect to the aging or storage time up to nearly 2 months. There was no obvious degradation of the sample's hydrophobicity was observed within this period.

So as to examine the effect of oxygen content, the ratio of oxygen to TMS in Ar carrier was varied with an expectation to form SiO_2-like thin film. The dependence of WCA on the O_2/TMS ratio is shown in Fig. 6. The TMS concentration, total gas flow rate, applied voltage and deposition time were fixed constant at 0.7 v/v%, 1.0 L min^{-1}, 16 kV and 5 min, respectively. As seen, the WCA rapidly decreased with increasing the O_2/TMS ratio from 0 to 8. The decrease of WCA was due to the incorporation of oxygen species into the coating network, which will be shown in the next section by the FTIR characterization. The WCA, however, did not further

http://dx.doi.org/10.1016/j.heliyon.2018.e00522
2405-8440/© 2018 The Authors. Published by Elsevier Ltd. This is an open access article under the CC BY-NC-ND license (http://creativecommons.org/licenses/by-nc-nd/4.0/).

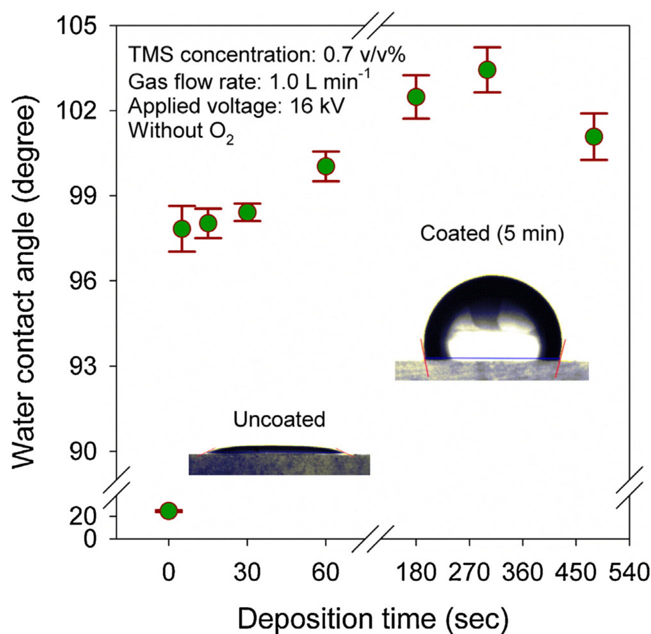

Fig. 4. Time dependence of WCA of hydrophobically treated samples (gas flow rate: 1.0 L min^{-1}, TMS concentration: 0.7 v/v%, applied voltage: 16 kV).

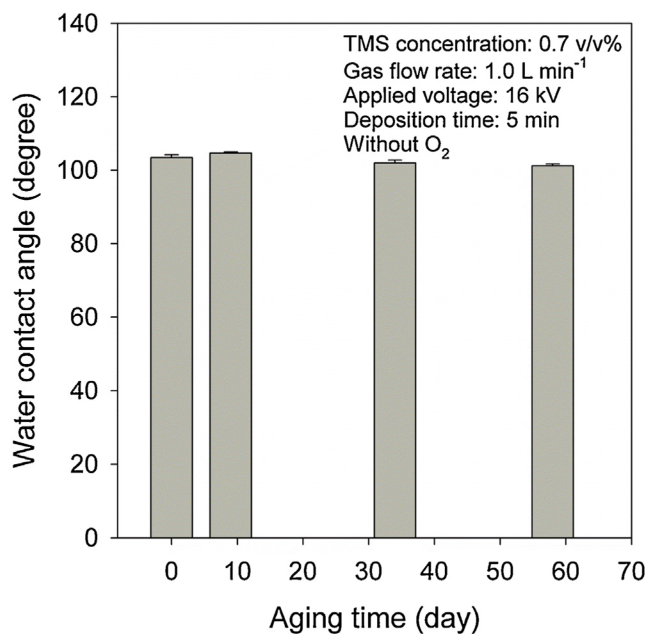

Fig. 5. Aging effect on WCA of the hydrophobically coated sample (gas flow rate: 1.0 L min^{-1}, TMS concentration: 0.7 v/v%, applied voltage: 16 kV, deposition time: 5 min).

http://dx.doi.org/10.1016/j.heliyon.2018.e00522
2405-8440/© 2018 The Authors. Published by Elsevier Ltd. This is an open access article under the CC BY-NC-ND license (http://creativecommons.org/licenses/by-nc-nd/4.0/).

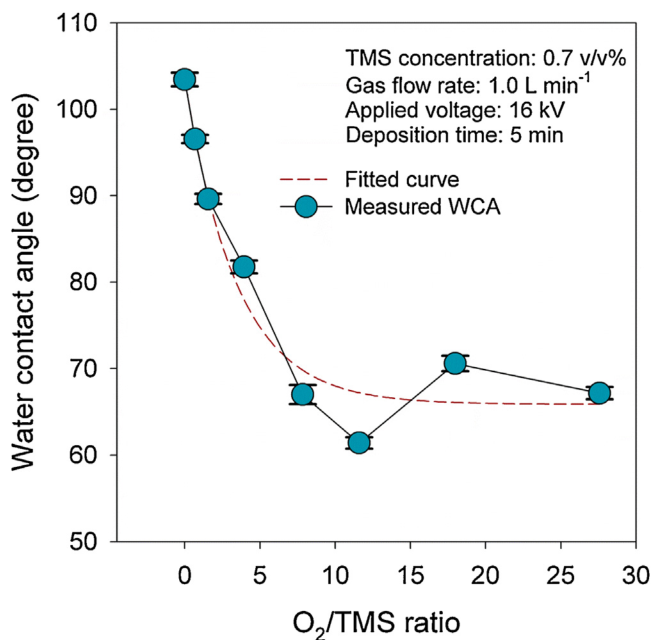

Fig. 6. O_2/TMS ratio dependence of WCA (total gas flow rate: 1.0 L min^{-1}, TMS concentration: 0.7 v/v%, applied voltage: 16 kV, deposition time: 5 min).

decrease as the O_2/TMS ratio higher than 8. At these high values of O_2/TMS ratio, the WCA remained at around 67°. This behavior suggests that the non-polar groups, namely methyl groups, still existed to some extent regardless of oxygen content. The SiO_2-like coating was therefore not successfully formed under the conditions of low power frequency and atmospheric pressure. The reasons are probably the low concentration and short lifetime of plasma-induced active oxygen species under these conditions compared to those in the low pressure, high power plasmas.

3.2. FTIR, XPS and AFM characterizations

Fig. 7 shows the FTIR spectra of the treated glass obtained by varying the deposition time at a TMS concentration of 0.7 v/v%, without (Fig. 7(a)) and with oxygen (Fig. 7(b)). The "0 s" implied the pristine glass whose IR spectrum was added for comparison. As seen, the used glass was transparent only in the range of 2500 and 4000 cm^{-1}. When the coating was formed on the substrate, a new peak appeared at around 2960 cm^{-1}, being assigned to the antisymmetric stretching of CH_3 groups, which were responsible for the hydrophobicity of the coatings [36, 37]. In the absence of oxygen, the peak intensity of this non-polar group increased gradually with the deposition time, obviously due to the increase in the coating thickness. At the constant deposition time of 5 min, the addition of oxygen (Fig. 7(b)) did not result in the elimination of CH_3 groups, suggesting that plasma-induced oxygen species was involved mainly in combination with Si in the

http://dx.doi.org/10.1016/j.heliyon.2018.e00522
2405-8440/© 2018 The Authors. Published by Elsevier Ltd. This is an open access article under the CC BY-NC-ND license (http://creativecommons.org/licenses/by-nc-nd/4.0/).

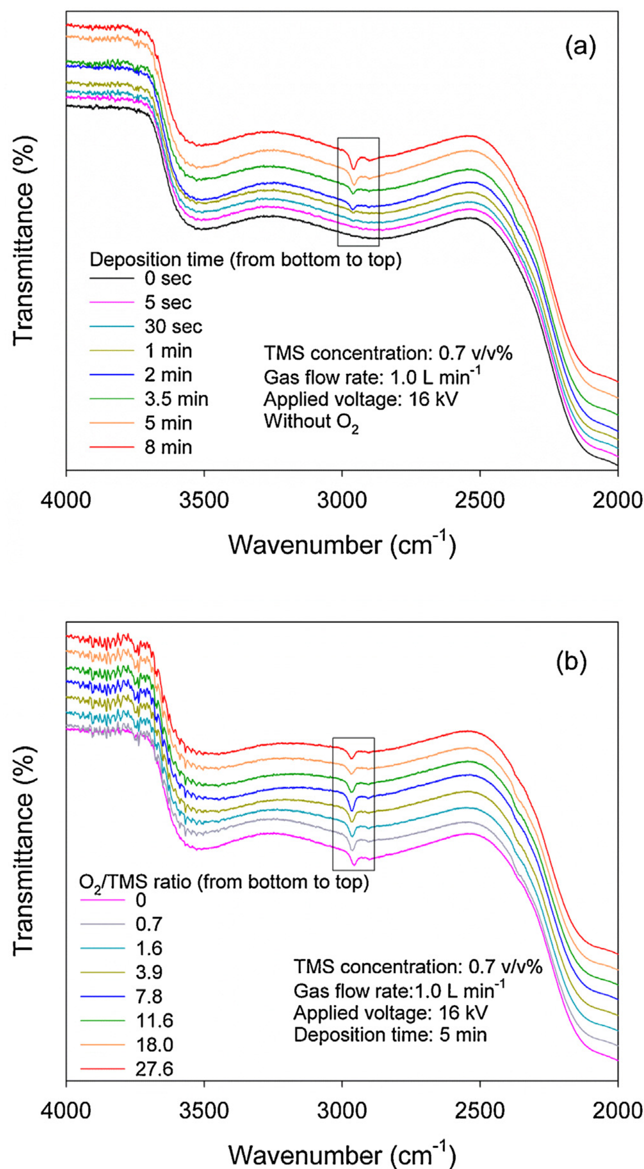

Fig. 7. FTIR spectra of coated samples obtained by varying deposition time (without oxygen, TMS concentration: 0.7 v/v%) (a) and by varying O_2/TMS ratio (TMS concentration: 0.7 v/v%, deposition time: 5 min) (b).

coating's backbone, which was not observed due to the strong absorption of the glass substrate in the range from 400 to 2000 cm^{-1}. The results are consistent with the WCA measurement shown in Fig. 6 since the WCA stayed above 65°, regardless of the high oxygen content. The retaining of methyl groups, on the other hand, could be beneficial for the $SiO_xC_yH_z$ thin film acting as the silicon oxide-based low dielectric material [38]. Differently, as revealed from literature, the addition of oxygen in the low-pressure, microwave and RF plasmas largely

http://dx.doi.org/10.1016/j.heliyon.2018.e00522
2405-8440/© 2018 The Authors. Published by Elsevier Ltd. This is an open access article under the CC BY-NC-ND license (http://creativecommons.org/licenses/by-nc-nd/4.0/).

reduced CH_3 groups of TMS-based coatings, leading to the formation of SiO_x-like films [29, 39, 40].

The TMS-based films were then deposited on KBr discs (diameter: 13 mm, thickness: 1.4 mm), which are fully IR-transparent, for a better understanding of their chemical structures. Three coated samples were prepared at a TMS concentration of 0.7 v/v% without and with oxygen (O_2/TMS ratio: 7.8), and the applied voltage was fixed at 14 kV for all cases. The coated samples were named as (b) TMS(5 min), (c) TMS(20 min) and (d) TMS + O_2(5 min) in Fig. 8, where the time values shown in the parenthesis are the deposition time. Samples (a) pristine and (e) gaseous TMS are the bare KBr and gaseous TMS diluted in Ar gas, respectively. The spectrum of sample (e) was not successfully taken from 400 and 950 cm^{-1}, due to the strong IR absorption of the CaF_2 gas-cell windows in this range. Compared to the bare KBr's spectrum, several new absorption bands in the region of 500 and 1500 cm^{-1} along with one of CH_3 groups at around 2960 cm^{-1} are observed for the all coated samples. The peak wavenumbers and their respective assignments are shown in Table 1. Among detected groups, CH_3 and $Si(CH_3)_x$ were obviously originated from the TMS monomer. Meanwhile, the $Si(CH_2)_nSi$ network of the pure TMS coating (sample (b) or (c)) appearing as a very strong band at around 1030 cm^{-1} was formed in plasma [41], initiated by the hydrogen abscission from methyl groups by energetic electrons and active excited Ar species. The gaseous TMS, sample (e), has no characteristic band in this region.

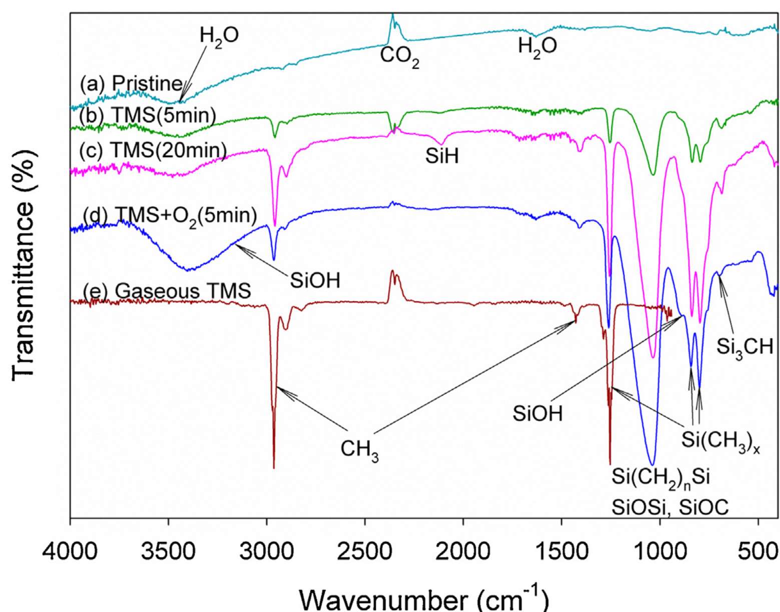

Fig. 8. FTIR spectra of bare KBr (a); coated KBr without oxygen, deposition time of 5 min (b), 20 min (c); with oxygen (O_2/TMS ratio: 7.8, deposition time: 5 min) (d) and gaseous TMS (e) (plasma coating performed at TMS concentration of 0.7 v/v% and applied voltage: 14 kV).

http://dx.doi.org/10.1016/j.heliyon.2018.e00522
2405-8440/© 2018 The Authors. Published by Elsevier Ltd. This is an open access article under the CC BY-NC-ND license (http://creativecommons.org/licenses/by-nc-nd/4.0/).

Table 1. IR wavenumbers and assignments of main absorption bands of coated samples and TMS monomer.

Assignments Samples	H_2O, SiOH Wavenumber (cm^{-1})	CH_3	SiH	$Si(CH_3)_x$	$Si(CH_2)_nSi$, SiOSi	Si_3CH
TMS(5 min)	1634, 3445	1411, 2957	2120	794, 836, 1254	1031	686
TMS(20 min)	1632/3478	1410, 2959	2111	795, 838, 1256	1035	686
TMS + O_2(5 min)	886, 1630, 3401	1409, 2963	–	799, 842, 1260	1037	697
Gaseous TMS	–	1428, 2963	–	1253	–	–
Ref.	[37]	[33]	[38]	[14, 38, 39, 40]	[26, 38, 41]	[42]

As oxygen was added, the main peaks at 2960, 1260 and especially at around 1030 cm^{-1} were strongly promoted. The peak intensification at around 1030 cm^{-1} was probably due to the formation of SiOSi and/or SiOC linkages, which also fall in this region along with the $Si(CH_2)_nSi$ network [42]. It is noted that the peak area ratio between the band at 1030 cm^{-1} and the one at 2960 cm^{-1} (*i.e.*, CH_3 groups) for the pure TMS coatings (samples (b) and (c)) is about 5; however, the figure for the TMS + O_2 coating (sample (d)) is much larger, of about 19. This suggests that when oxygen was added, the absorption band at around 1030 cm^{-1} was mainly induced by the SiOSi and/or SiOC rather than the $Si(CH_2)_nSi$ backbone. In addition, a strong, broad band at around 3400 cm^{-1} observed from the sample (d) is assigned to the stretching of SiOH bonds that caused a strong shoulder at 886 cm^{-1} [43]. Meanwhile, the faint peaks located at a little higher than 3400 cm^{-1} from the samples (a), (b) and (c) are due to water adsorbed on the KBr pellets. For all coated samples, a weak band at around 690 cm^{-1} could be attributed to Si_3CH configuration, characterizing the stretching motion of carbon with its neighboring hydrogen and silicon atoms [44]. As the deposition time increased from 5 to 20 min, without oxygen, the stretching mode of SiH units was observed at 2111 cm^{-1} (sample (c)), which was also detected in a previous work for the samples prepared with no or relatively low oxygen concentrations [42].

Table 2. Atomic percentage of Si, C and O from XPS for two coatings with different O_2/TMS ratios of 0 and 11.6 (TMS: 0.7 v/v%, gas flow rate: 1.0 L min^{-1}, applied voltage: 16 kV and deposition time: 5 min).

O_2/TMS ratio	Atomic percentage (%)		
	Si	C	O
0	19.4	55.9	22.6
11.6	26.8	36.2	36.7

http://dx.doi.org/10.1016/j.heliyon.2018.e00522
2405-8440/© 2018 The Authors. Published by Elsevier Ltd. This is an open access article under the CC BY-NC-ND license (http://creativecommons.org/licenses/by-nc-nd/4.0/).

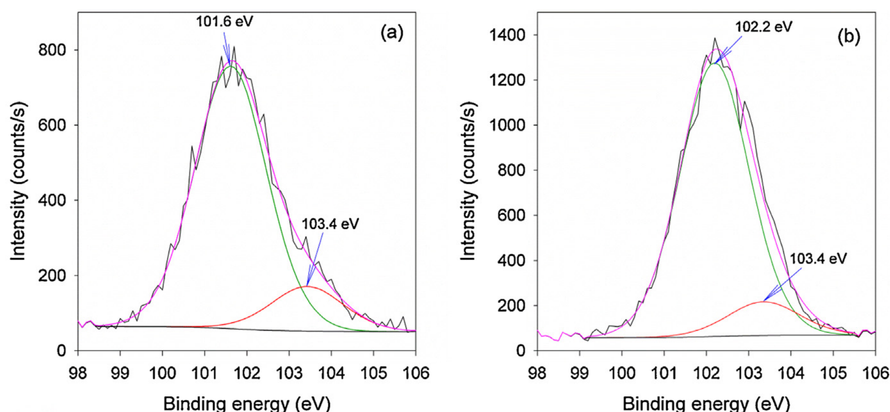

Fig. 9. High-resolution XPS spectra of Si_{2p} peaks for the coatings with the O_2/TMS ratio of (a) 0 and (b) 11.6 (TMS: 0.7 v/v%, gas flow rate: 1.0 L min^{-1}, applied voltage: 16 kV and deposition time: 5 min).

The results of XPS analysis were shown in Table 2 and Fig. 9. As seen from Table 2, by adding oxygen to the discharge gas mixture, the content of C in the coating significantly decreased from 55.9 to 36.2%. Meanwhile, the figure for O increased from 22.6 to 36.7%. These changes in C and O content are due to the oxidation and removal of C_xH_y groups by the plasma-induced active oxygen species. However, C was not completely removed when oxygen was added. The source of O in the sample of zero O_2/TMS ratio was probably the oxygen that preexisted in the plasma chamber. Fig. 9 shows the Si_{2p} spectra of the two samples listed in Table 2. The Si_{2p} peak shifted from 101.7 to 102.3 eV as additional oxygen was fed to the reactor. The deconvoluted spectra of Si_{2p} indicate that the silicon chemical bond of $(R)_3{-}Si{-}(O)_1$ at 101.6 eV mainly existed in the TMS coating (Fig. 9(a)), where R represents carbon and hydrogen-containing partial structure [45, 46]. Meanwhile, when additional oxygen was introduced, C was further replaced by O, leading to the transformation of $(R)_3{-}Si{-}(O)_1$ chemical bond to $(R)_2{-}Si{-}(O)_2$ chemical bond which appeared at around 102.2 eV. In addition, a peak of $Si{-}(O)_4$ structure at a higher binding energy of 103.2 eV was observed on both coatings' spectra (Fig. 9(a) and (b)). The coatings were, however, still composed of a large portion of the organic $(R)_3{-}Si{-}(O)_1$ and $(R)_2{-}Si{-}(O)_2$ components, which is consistent with the FTIR analysis.

The surface morphology of pristine glass and plasma-treated ones, performed by AFM technique, are shown in Fig. 10. The hydrophobically coated glass (Fig. 10(b) and (c)) is observed to have a uniform, smooth surface with a root mean square roughness, R_q, of 1.481 nm. This surface morphology is consistent with the WCA of around 100°. Besides chemical composition, morphology is an important factor in determining the wettability of a solid surface. Super-hydrophobicity (WCA $\geq$ 150°) requires a surface that is both hydrophobic and

http://dx.doi.org/10.1016/j.heliyon.2018.e00522
2405-8440/© 2018 The Authors. Published by Elsevier Ltd. This is an open access article under the CC BY-NC-ND license (http://creativecommons.org/licenses/by-nc-nd/4.0/).

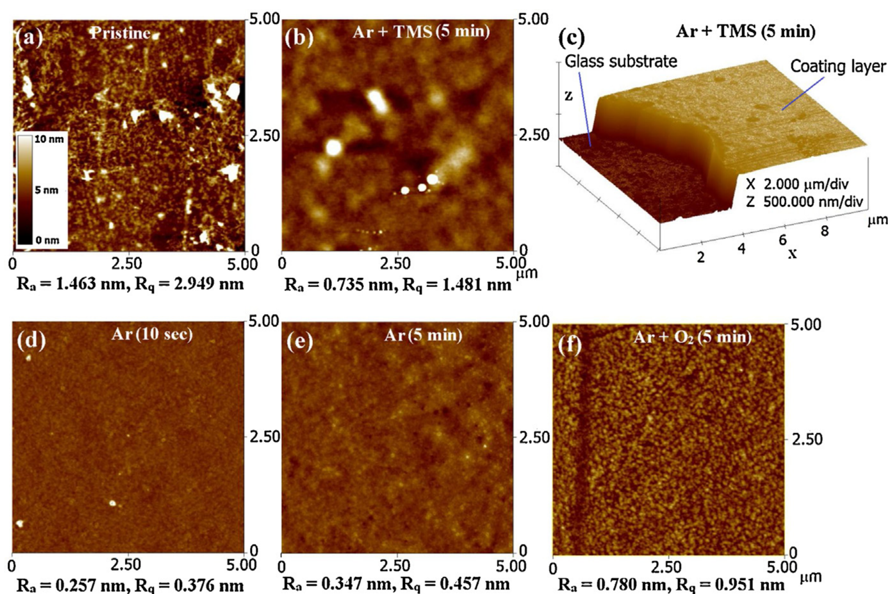

Fig. 10. Surface morphology of glass samples by AFM without treatment (a); hydrophobically treated at TMS concentration of 0.7 v/v% and applied voltage of 16 kV for 5 min (b) and (c); hydrophilically treated at applied voltage of 9 kV with Ar plasma for 10 s (d), 5 min (e); and with O_2/Ar plasma for 5 min (f).

rough at the sub-microscale, often obtained by atmospheric RF, high-density plasma, which allows solid particulates to form in the gas phase [14, 17]. By partially removing the coating using a razor blade, the coating thickness was estimated to be 0.32 μm. For surface cleaning, after 10 s of Ar plasma exposure (Fig. 10(d)), the large, high islands existing on the pristine glass surface were removed, leaving a flat surface with a very small R_q of 0.376 nm. This change in surface morphology resulted from the removal of organic contaminants taking place in the plasma discharges by the ionic and photonic bombardment [47]. It clearly shows that the DDBD plasma at low input power is also effective for surface cleaning and capable of replacing the commonly used chemical methods. Raising the deposition time to 5 min resulted in a similar surface pattern with a slightly increased roughness compared to the case of short-time exposure. When oxygen was added (Fig. 10(f)), the surface roughening was, however, more significant with small grains densely appearing on the surface, being attributed to the oxidation of the alkaline elements of the glass, which was observed in a previous study [48].

4. Conclusions

A double-dielectric barrier discharge reactor energized by an AC, 400-Hz-frequency power source at atmospheric pressure was used for tailoring the wettability of glass. The hydrophobic transformation of glass surfaces was

http://dx.doi.org/10.1016/j.heliyon.2018.e00522
2405-8440/© 2018 The Authors. Published by Elsevier Ltd. This is an open access article under the CC BY-NC-ND license (http://creativecommons.org/licenses/by-nc-nd/4.0/).

performed by plasma polymerization of TMS monomer (in Ar gas). Both deposition time and applied voltage had a positive effect on the hydrophobicity of the coated glass. The resulting polymerized film was uniform and had a smooth surface with the highest WCA of about 106°, similar to those previously reported in the literature using low-pressure, RF plasmas. The addition of oxygen, however, did not result in the formation of SiO_2-like coatings as methyl groups were observed to be retained, regardless of oxygen content.

Declarations

Author contribution statement

Quang Hung Trinh: Conceived and designed the experiments; Performed the experiments; Wrote the paper.

Young Sun Mok: Conceived and designed the experiments; Analyzed and interpreted the data; Contributed reagents, materials, analysis tools or data.

Md. Mokter Hossain: Performed the experiments.

Seong H. Kim: Analyzed and interpreted the data.

Competing interest statement

The authors declare no conflict of interest.

Funding statement

This work was supported by the research grant of Jeju National University in 2015.

Additional information

No additional information is available for this paper.

References

[1] Q.H. Trinh, Y.S. Mok, Environmental plasma-catalysis for the energy-efficient treatment of volatile organic compounds, Korean J. Chem. Eng. 33 (2016) 735–748.

[2] J. Friedrich, Mechanisms of plasma polymerization – reviewed from a chemical point of view, Plasma Processes Polym. 8 (2011) 783–802.

[3] K.G. Kostov, R.Y. Honda, L.M.S. Alves, M.E. Kayama, Characteristics of dielectric barrier discharge reactor for material treatment, Braz. J. Phys. 39 (2009) 322–325.

 http://dx.doi.org/10.1016/j.heliyon.2018.e00522
2405-8440/© 2018 The Authors. Published by Elsevier Ltd. This is an open access article under the CC BY-NC-ND license (http://creativecommons.org/licenses/by-nc-nd/4.0/).

[4] Y.L. Cheng, Y.K. Wang, P. Chen, S.B. Deng, R. Ruan, Non-thermal plasma assisted polymer surface modification and synthesis: a review, Int. J. Agric. Biol. Eng. 7 (2014) 1–9.

[5] A. Pamreddy, D. Skácelová, M. Haničinec, P. Sťahel, M. Stupavská, M. Černák, et al., Plasma cleaning and activation of silicon surface in dielectric coplanar surface barrier discharge, Surf. Coat. Technol. 236 (2013) 326–331.

[6] V. Raballand, J. Benedikt, S. Hoffmann, M. Zimmermann, A. von Keudell, Deposition of silicon dioxide films using an atmospheric pressure microplasma jet, J. Appl. Phys. 105 (2009) 083304.

[7] R. Thyen, A. Weber, C.-P. Klages, Plasma-enhanced chemical-vapour-deposition of thin films by corona discharge at atmospheric pressure, Surf. Coat. Technol. 97 (1997) 426–434.

[8] K.V. Rani, N. Chandwani, P. Kikani, S.K. Nema, A.K. Sarma, B. Sarma, Hydrophobic surface modification of silk fabric using plasma-polymerized HMDSO, Surf. Rev. Lett. 25 (2018) 1850060.

[9] J.-H. Kim, G. Liu, S.H. Kim, Deposition of stable hydrophobic coatings with in-line CH_4 atmospheric rf plasma, J. Mater. Chem. 16 (2006) 977–981.

[10] M.D. Barankin, E. Gonzalez II, S.B. Habib, L. Gao, P.C. Guschl, R.F. Hicks, Hydrophobic films by atmospheric plasma curing of spun-on liquid precursors, Langmuir 25 (2009) 2495–2500.

[11] R. Múgica-Vidal, F. Alba-Elías, E. Sainz-García, M. Pantoja-Ruiz, Hydrophobicity attainment and wear resistance enhancement on glass substrates by atmospheric plasma-polymerization of mixtures of an aminosilane and a fluorocarbon, Appl. Surf. Sci. 347 (2015) 325–335.

[12] Z. Fang, Y. Qui, H. Wang, E. Kuffel, Improving hydrophobicity of glass surface using dielectric barrier discharge treatment in atmospheric air, Plasma Sci. Technol. 9 (2007) 582–586.

[13] C. Wang, X. He, Preparation of hydrophobic coating on glass surface by dielectric barrier discharge using a 16 kHz power supply, Appl. Surf. Sci. 252 (2006) 8348–8351.

[14] S.H. Lee, Z.R. Dilworth, E. Hsiao, A.L. Barnette, M. Marino, J.H. Kim, J.G. Kang, T.H. Jung, S.H. Kim, One-step production of superhydrophobic coatings on flat substrates via atmospheric RF plasma process using non-fluorinated hydrocarbons, ACS Appl. Mater. Interfaces 3 (2011) 476–481.

 http://dx.doi.org/10.1016/j.heliyon.2018.e00522
2405-8440/© 2018 The Authors. Published by Elsevier Ltd. This is an open access article under the CC BY-NC-ND license (http://creativecommons.org/licenses/by-nc-nd/4.0/).

[15] H.H. Son, J.N. Park, W.G. Lee, Hydrophobic properties of films grown by torch-type atmospheric pressure plasma in Ar ambient containing C6 hydrocarbon precursor, Korean J. Chem. Eng. 30 (2013) 1480–1484.

[16] Y.-Y. Ji, S.-S. Kim, O.-P. Kwon, S.-H. Lee, Easy fabrication of large-size superhydrophobic surfaces by atmospheric pressure plasma polymerization with non-polar aromatic hydrocarbon in an in-line process, Appl. Surf. Sci. 255 (2009) 4575–4578.

[17] D.J. Marchand, Z.R. Dilworth, R.J. Stauffer, E. Hsiao, J.-H. Kim, J.-G. Kang, S.H. Kim, Atmospheric rf plasma deposition of superhydrophobic coatings using tetramethylsilane precursor, Surf. Coat. Technol. 234 (2013) 14–20.

[18] V. Štěpánová, P. Slavíček, M. Valtr, V. Buršíková, M. Stupavská, Improvement of glass wetability using diffuse coplanar surface barrier discharge and gliding arc considerig aging effect, 7th Int. Conf. Nanomaterials (Nanocon 2015), Brno, Czek Republic, Oct. 14–16, 2015, pp. 2–7.

[19] T. Homola, J. Matoušek, M. Kormunda, L.Y.L. Wu, M. Černák, Plasma treatment of glass surfaces using diffuse coplanar surface barrier discharge in ambient air, Plasma Chem. Plasma Process. 33 (2013) 881–894.

[20] R.R. Elfa, M.K. Ahmad, N. Nafarizal, M.Z. Sahdan, C.F. Soon, Hydrophilic property of glass treated by needle plasma jet for surface modification, 2016 IEEE Int. Conf. Semicond. Electron., Kuala Lumpur, Malaysia, Aug. 17–19, 2016, pp. 212–215.

[21] S.M. Hong, S.H. Kim, Jeong H. Kim, H.I. Hwang, Hydrophilic surface modification of PDMS using atmospheric RF Plasma, J. Phys. Conf. Ser. 34 (2006) 656–661.

[22] K.-S. Seo, J.-H. Cha, M.-K. Han, C.-S. Ha, D.-H. Kim, H.J. Lee, H.-J. Lee, Surface treatment of glass and poly(dimethylsiloxane) using atmospheric-pressure plasma jet and analysis of discharge characteristics, Jpn. J. Appl. Phys. 54 (2015) 01AE06.

[23] S.H. Tan, N.-T. Nguyen, Y.C. Chua, T.G. Kang, Oxygen plasma treatment for reducing hydrophobicity of a sealed polydimethylsiloxane microchannel, Biomicrofluidics 4 (2010) 032204.

[24] A.K. Riau, D. Mondal, G.H.F. Yam, M. Setiawan, B. Liedberg, S.S. Venkatraman, J.S. Mehta, Surface modification of PMMA to improve adhesion to corneal substitutes in a synthetic core-skirt keratoprosthesis, ACS Appl. Mater. Interfaces 7 (2015) 21690–21702.

[25] Á. Yanguas-Gil, Á. Barranco, J. Cotrino, P. Gröning, A.R. Gonzalez-Elipe, Plasma characterization of oxygen-tetramethylsilane mixtures for the plasma-

2405-8440/© 2018 The Authors. Published by Elsevier Ltd. This is an open access article under the CC BY-NC-ND license (http://creativecommons.org/licenses/by-nc-nd/4.0/).

enhanced CVD of $SiO_xC_yH_z$ thin films, Chem. Vap. Depos. 12 (2006) 728–735.

[26] A.M. Wrobel, P. Uznanski, A. Walkiewicz-Pietrzykowska, B. Glebocki, E. Bryszewska, Silicon oxycarbide films produced by remote microwave hydrogen plasma CVD using a tetramethyldisiloxane precursor, Chem. Vap. Depos. 21 (2015) 307–318.

[27] K.-S. Chen, S.-C. Liao, S.-H. Tsao, N. Inagaki, H.-M. Wu, C.-Y. Chou, W.-Y. Chen, Deposition of tetramethylsilane on the glass by plasma-enhanced chemical vapor deposition and atmospheric pressure plasma treatment, Surf. Coat. Technol. 228 (2013) S33–S36.

[28] V. Raballand, J. Benedikt, S. Hoffmann, M. Zimmermann, A. Von Keudell, Deposition of silicon dioxide films using an atmospheric pressure microplasma jet, J. Appl. Phys. 105 (2009) 083304.

[29] M. Kihel, S. Sahli, A. Zenasni, P. Raynaud, Y. Segui, Dielectric properties of SiO_x like films deposited from TMS/O_2 mixture in low pressure microwave plasma, Vacuum 107 (2014) 264–268.

[30] A. Rousseau, A. Dantier, L. Gatilova, Y. Ionikh, J. Röpcke, Y. Tolmachev, On NO_x production and volatile organic compound removal in a pulsed microwave discharge in air, Plasma Sources Sci. Technol. 14 (70) (2005).

[31] H. Kim, A. Ogata, S. Futamura, Effect of different catalysts on the decomposition of VOCs using flow-type plasma-driven catalysis, IEEE Trans. Plasma Sci. 34 (2006) 984–995.

[32] N. Tenn, K. Fatyeyeva, J. Valleton, F. Poncin-epaillard, N. Delpouve, Improvement of water barrier properties of poly (ethylene-co-vinyl alcohol) films by hydrophobic plasma surface treatments, J. Phys. Chem. C 116 (2012) 12599–12612.

[33] S. Yeo, T. Kwon, C. Choi, H. Park, J.W. Hyun, D. Jung, The patterned hydrophilic surfaces of glass slides to be applicable for the construction of protein chips, Curr. Appl. Phys. 6 (2006) 267–270.

[34] J.E. Jones, M. Chen, Q. Yu, Corrosion resistance improvement for 316L stainless steel coronary artery stents by trimethylsilane plasma nanocoatings, J. Biomed. Mater. Res. B Appl. Biomater. 102 (2014) 1363–1374.

[35] R. Morent, N. De Geyter, S. Van Vlierberghe, P. Dubruel, C. Leys, E. Schacht, Organic-inorganic behaviour of HMDSO films plasma-polymerized at atmospheric pressure, Surf. Coat. Technol. 203 (2009) 1366–1372.

 http://dx.doi.org/10.1016/j.heliyon.2018.e00522
2405-8440/© 2018 The Authors. Published by Elsevier Ltd. This is an open access article under the CC BY-NC-ND license (http://creativecommons.org/licenses/by-nc-nd/4.0/).

[36] F. Scheinmann, An Introduction to Spectroscopic Methods for the Identification of Organic Compounds, Pergamon Press, Oxford, 1970.

[37] S. Gunasekaran, S. Ponnusamy, Vibrational spectra and normal coordinate analysis on an organic non-linear optical crystal-3-methoxy-4-hydroxy benzaldehyde, Indian J. Pure Appl. Phys. 43 (2005) 838–843.

[38] S.-Y. Jing, C.K. Choi, H.-J. Lee, A study on the formation and characteristics of the organic-inorganic material with low dielectric constant deposited by high density plasma chemical vapor deposition, J. Korean Phys. Soc. 39 (2001) S302–S305.

[39] T. Matsuda, M. Furuta, T. Hiramatsu, H. Furuta, T. Kawaharamura, T. Hirao, Low temperature deposition of SiO_x insulator film with newly developed facing electrodes chemical vapor deposition, Vacuum 101 (2014) 189–192.

[40] C.-Y. Wu, R.-M. Liao, L.-W. Lai, M.-S. Jeng, D.-S. Liu, Organosilicon/silicon oxide gas barrier structure encapsulated flexible plastic substrate by using plasma-enhanced chemical vapor deposition, Surf. Coat. Technol. 206 (2012) 4685–4691.

[41] K. Teshima, Y. Inoue, H. Sugimura, O. Takai, Growth and structure of silica films deposited on a polymeric material by plasma-enhanced chemical vapor deposition, Thin Solid Films 420–421 (2002) 324–329.

[42] A. Walkiewicz-Pietrzykowska, J.P. Espinós, A.R. González-Elipe, Type of precursor and synthesis of silicon oxycarbide (SiOxCyH thin films with a surfatron microwave oxygen/argon plasma, J. Vac. Sci. Technol. A Vac. Surf. Films 24 (2006) 988.

[43] L. Calabrese, L. Bonaccorsi, A. Caprì, E. Proverbio, Enhancement of the mechanical properties of a zeolite based composite coating on an aluminum substrate by silane matrix modification, Ind. Eng. Chem. Res. 55 (2016) 6952–6960.

[44] A. Kleinová, J. Huran, V. Sasinková, M. Perný, V. Šály, J. Packa, FTIR spectroscopy of silicon carbide thin films prepared by PECVD technology for solar cell application, Proc. SPIE 9563 (2015) 95630U1-95630U-8.

[45] Y.-S. Lin, C.-L. Chen, Wear resistance of low-temperature plasma-polymerized organosilica deposited on poly(ethylene terephthalate): the effect of discharge powers, J. Appl. Polym. Sci. 110 (2008) 2704–2710.

[46] Y.-S. Lin, C.-L. Chen, Wear resistance of low-temperature Plasma-polymerized organosilica deposited on poly (ethylene terephthalate): the effect of O_2 addition, Plasma Processes Polym. 3 (2006) 650–660.

 http://dx.doi.org/10.1016/j.heliyon.2018.e00522
2405-8440/© 2018 The Authors. Published by Elsevier Ltd. This is an open access article under the CC BY-NC-ND license (http://creativecommons.org/licenses/by-nc-nd/4.0/).

[47] M. Avram, A.M. Avram, A. Bragaru, A. Ghiu, C. Iliescu, Plasma surface modification for selective hydrophobic control, Roman. J. Inf. Sci. Technol. 11 (2008) 409–422.

[48] A.U. Alam, M.M.R. Howlader, M.J. Deen, Oxygen plasma and humidity dependent surface analysis of silicon, silicon dioxide and glass for direct wafer bonding, ECS J. Solid State Sci. Technol. 2 (2013) P515–P523.

http://dx.doi.org/10.1016/j.heliyon.2018.e00522
2405-8440/© 2018 The Authors. Published by Elsevier Ltd. This is an open access article under the CC BY-NC-ND license (http://creativecommons.org/licenses/by-nc-nd/4.0/).